Journal of Materials Chemistry A

RSC Publishing

PAPER

View Article Online
View Journal | View Issue

Cite this: J. Mater. Chem. A, 2013, 1, 11043

One-dimensional channel-structured Eu-MOF for sensing small organic molecules and Cu^{2+} ion†

Zhaomin Hao,[ab] Xuezhi Song,[ab] Min Zhu,[ab] Xing Meng,[ab] Shuna Zhao,[ab] Shengqun Su,[ab] Weiting Yang,[a] Shuyan Song[a] and Hongjie Zhang*[a]

Received 12th June 2013
Accepted 12th July 2013

DOI: 10.1039/c3ta12270k

www.rsc.org/MaterialsA

Two new lanthanide metal–organic frameworks Ln(FBPT)(H_2O)(DMF) (FBPT = 2′-fluoro-biphenyl-3,4′,5-tricarboxylate, Ln = Eu and Tb) were prepared under solvothermal conditions. Single crystal X-ray diffraction analyses reveal that the two compounds are isostructurally related with the same one-dimensional channel structure on the basis of FBPT as an organic linker. Herein, the Eu(FBPT)(H_2O)(DMF) (**EuL**) is selected as a representative sample for luminescent measurements. Study of the photoluminescence properties reveals that the **EuL** exhibits red emission, corresponding to the $^5D_0 \rightarrow {}^7F_J$ (J = 1–4) transitions of the Eu^{3+} ion under UV light excitation. Most interestingly, when this compound was immersed in the different organic solvents and metal ion DMF solutions, it shows highly selective and sensitive sensing for small organic molecules and Cu^{2+} ions. In connection to this, a probable sensing mechanism was also discussed in this paper.

1 Introduction

Over the last two decades, extensive efforts on metal–organic frameworks (MOFs) have not only led to the creation of a huge number of diverse topologies with aesthetic beauty, but also initiated rational design strategies to construct porous materials with high surface areas, predictable structure, and tunable pore sizes for use in some important applications, such as gas storage, separation, heterogeneous catalysis, sensing and drug delivery.[1–7] Among the diverse MOFs, microporous lanthanide metal–organic frameworks (Ln-MOFs) are well known for their unique optical and magnetic properties, as well as their characteristic coordination preferences.[8] Taking advantage of the optical properties, microporous Ln-MOFs possess lots of fascinating features, such as Stokes' shifts, high color purity, and relatively long luminescence lifetimes, which originate from f–f transitions *via* an "antenna effect" can be investigated.[9–11] These optical properties of microporous Ln-MOFs make them especially attractive for potential applications in fluorescence probes and luminescence bioassays.[12] Meanwhile, such progress in the optical properties of microporous Ln-MOFs also guides and inspires us to rationally design and synthesize more characteristic microporous Ln-MOFs for host–guest recognition and to tune their functional properties, however, it is still a challenge to get the desired microporous Ln-MOFs. This is because lanthanide ions have a larger coordination sphere and more flexible coordination geometry, and the open lanthanide sites formed *in situ* during activation/de-solvation tend to bind back with the oxygen and/nitrogen donors from the organic linkers to form a condensed structure.

Nonetheless, the above problems did not deter researchers from exploring the luminescent microporous Ln-MOFs for their sensing applications. Over the past few years, a wide range of luminescent lanthanide-based MOFs, for sensing cations, anions, small molecules and vapors have been realized and reported by Chen, Lee, Harbuzaru and Liu *et al.*[13] In fact, to make use of the luminescent Ln-MOFs for the unique recognition of small molecules and cations, our group have also recently realized a few microporous luminescent Ln-MOFs for sensing applications.[14] Throughout recent years, we have been constantly dedicated to expanding and improving the luminescent microporous Ln-MOFs for their sensing applications. As far as we know, reports about fluorinated microporous Ln-MOFs as luminescent probes for sensing small organic molecules and metal ions are still relatively rare. Herein, we present a fluorinated luminescent material Eu(FBPT)(H_2O)(DMF) (**EuL**) as a highly selective fluorescent probe targeting small organic molecules and Cu^{2+} ions, and the possible sensing mechanism is also discussed.

2 Experimental

2.1 Materials and measurements

All chemicals were commercially available and used as received without further purification. Scheme S1† shows the

[a]State Key Laboratory of Rare Earth Resource Utilization, Changchun Institute of Applied Chemistry, Chinese Academy of Sciences, Changchun 130022, People's Republic of China. E-mail: hongjie@ciac.jl.cn; Fax: +86 43185685653; Tel: +86 43185262127

[b]Graduate University of Chinese Academy of Sciences, Beijing, 100049, People's Republic of China

† Electronic supplementary information (ESI) available. CCDC 923447 and 923448. For ESI and crystallographic data in CIF or other electronic format see DOI: 10.1039/c3ta12270k

synthetic route to the ligand FBPT. Elemental analyses of the C, H, N, and Ln ions were carried out on a VarioEL analyzer (Elementar Analysensysteme GmbH) and *via* inductively coupled plasma (ICP) atomic emission spectrometric analysis (POEMS, TJA), respectively. ^{1}H NMR spectra were recorded on a Mercury Plus-400 spectrometer in DMSO-d^6. Mass spectra (MS) were run on a Thermo Scientific LXQ mass spectrometer equipped with an electrospray source. Absorption measurements were carried out using a Shimadzu UV-3600 spectrophotometer. XPS data was obtained using an ESCALAB 250 X-ray photoelectron spectrometer. Thermogravimetric analysis (TGA) was carried out using a SDT 2960 Simultaneous DSC-TGA of TA instruments up to 900 °C, and the heating rate was 10 °C min^{-1} under an air flow of 100 mL min^{-1}. Powder X-ray power diffraction (XRD) patterns were performed on a D8 Focus (Bruker) diffractometer with Cu-Kα radiation Field-emission (λ = 0.15405 nm, continuous, 40 kV, 40 mA, increment 0.02°).

2.2 Synthesis

Synthesis of 2′-fluoro-biphenyl-3,4′,5-tricarboxylate (FBPT). 1-Bromo-2-fluoro-4-methylbenzene (0.99 g, 5.275 mmol), 3,5-dimethylphenylboronic acid (0.95 g, 6.325 mmol) and tetrakis(triphenylphosphine)palladium^0 (0.19 g, 0.16 mmol) were dissolved in 20 mL of THF in a round-bottomed flask. After 15 mL of aqueous 2 M Na_2CO_3 was added, the reaction mixture was heated at 70 °C for 24 h under a nitrogen atmosphere. The cooled mixture was poured into water, extracted with CH_2Cl_2 (30 mL × 3 times) and then dried over anhydrous magnesium sulfate. Finally silica column purification (*n*-hexane as eluent) gave the product of 2′-fluoro-3,4′,5-trimethylbenzene (0.85 g, 3.96 mmol) with 75% yield. Then a mixture of 2′-fluoro-3,4′,5-trimethylbenzene (0.5 g), concentrated HNO_3 (1 mL) and deionized H_2O (8 mL) water was sealed in a 15 mL Teflon-lined stainless steel container. The container was heated to 160 °C and held at that temperature for 24 h, and then cooled to room temperature. Finally, a pale yellow product was obtained in 90% yield. ^{1}H NMR (400 MHz, DMSO-d^6, Fig. S1 in ESI†) δ = 13.51 (s, 3H), 8.72–8.49 (m, 1H), 8.46–8.27 (d, 2H), 8.01–7.67 (m, 3H). HRMS: calculated [M$^+$] 304.04; observed [M$^+$] 304.01.

Synthesis of EuL. FBPT (0.045 mmol, 13 mg), $Eu(NO_3)_3\cdot 6H_2O$ (0.045 mmol, 20 mg), DMF (2 mL), H_2O (1.3 mL) and ethanol (2 mL) were placed in a 10 mL glass vial, which was sealed and heated to 80 °C for 48 h, and then cooled to room temperature at a rate of 10 °C min^{-1}. The pH value of the reaction mixtures changed from 3.6 to 5.5. The colorless crystals formed were collected and air-dried (73% based on FBPT). Anal. calcd (%) for $C_{18}H_{15}EuFNO_8$ (M_r = 544.28): C, 39.72; H, 2.78; N, 2.57; Eu, 27.92. Found: C, 39.48; H, 3.09; N, 2.43; Eu, 28.22.

Synthesis of TbL. This compound was synthesized following the same synthetic procedure as that for compound **EuL** except that $Tb(NO_3)_3\cdot 6H_2O$ was used instead of $Eu(NO_3)_3\cdot 6H_2O$. Colorless crystals of **TbL** were obtained with 69% yield based on FBPT. Anal. calcd (%) for $C_{18}H_{15}TbFNO_8$ (M_r = 551.24): C, 39.22; H, 2.74; N, 2.54; Tb, 28.83. Found: C, 39.01; H, 2.93; N, 2.41; Tb, 28.56.

2.3 X-ray crystal structure determination

Suitable single crystals with dimensions of 0.24 × 0.21 × 0.19 mm^3 for **EuL** and 0.25 × 0.21 × 0.18 mm^3 for **TbL** were selected for single-crystal X-ray diffraction analyses. Crystallographic data was collected at 185 K on a Bruker Apex II CCD diffractometer with graphite monochromated Mo-Kα radiation (λ = 0.71073 Å). The crystal structure was deduced by means of direct methods and refined employing full-matrix least squares on F^2 (SHELXTL-97).[15] All the hydrogen atoms were generated geometrically and refined isotropically using the riding model. All non-hydrogen atoms were refined with anisotropic displacement parameters. In the compound **EuL**, the distance between C18 and N1 in the disordered DMF molecule was restrained (with the restraint command "DFIX") to a target value of 1.54 with an estimated standard deviation of 0.02. In the compound of **TbL**, a few lighter atoms (C and N) were restrained with the "ISOR" command due to their unreasonable anisotropic U_{eq} parameters and obvious ADP problems. These atoms are as follows: C16, C17, C18, N1. Furthermore, the bond length of C17–N1 in the disordered DMF molecule of compound **TbL** was also fixed with the restraint command "DFIX". In **EuL** and **TbL**, all these restrained commands led to the restraint number, but these treatments are necessary for the reasonable structural model. The crystal data and details of the structure determination for compounds **EuL** and **TbL** are listed in Table 1. Selected bond lengths and angles are given in Table 2.

Table 1 Crystal data collection and refinement details for **EuL** and **TbL**

Compound	**EuL**	**TbL**
Formula	$C_{18}H_{15}EuFNO_8$	$C_{18}H_{15}TbFNO_8$
M_r	544.28	551.24
Cryst. size, mm^3	0.24 × 0.21 × 0.19	0.25 × 0.21 × 0.18
Crystal system	Monoclinic	Monoclinic
Space group	*C*2/*c*	*C*2/*c*
a, Å	24.6841(13)	24.605(2)
b, Å	12.9554(7)	12.9653(12)
c, Å	14.6905(8)	14.6200(14)
β, deg	96.6580(10)	96.727(2)
Z	8	8
D_{calcd}, g cm^{-3}	1.549	1.575
F(000), e	2128	2144
hkl range	$-30 \le h \le 30$	$-18 \le h \le 29$
	$0 \le k \le 16$	$-15 \le k \le 15$
	$0 \le l \le 18$	$-14 \le l \le 17$
θ range, deg	1.66 to 26.05	1.67 to 25.00
Reflections collected/unique	4615/4604	11 186/4090
Data/restraints/parameters	4604/1/272	4090/33/272
GoF^a (F^2)	1.097	1.063
$R_1/\omega R_2$ [$I > 2\sigma(I)$]	R_1 = 0.0568	R_1 = 0.0597
	ωR_2 = 0.1636	ωR_2 = 0.1697
$R_1/\omega R_2{}^b$ (all data)	R_1 = 0.0675	R_1 = 0.0750
	ωR_2 = 0.1636	ωR_2 = 0.1793
Largest diff. peak/hole/e Å^{-3}	2.754 and −4.208	2.397 and −4.304

^{a} GoF = $[\Sigma\omega(F_o^2 - F_c^2)^2/(n_{obc} - n_{param})]^{1/2}$. ^{b} $R_1 = ||F_o| - |F_c||/\Sigma|F_o|$, $\omega R_2 = [\Sigma\omega(F_o^2 - F_c^2)^2/\Sigma\omega(F_o^2)^2]^{1/2}$.

2.4 Luminescent measurements

The luminescence spectra were recorded on a Hitachi F-4500 fluorescence spectrophotometer. The photomultiplier tube (PMT) voltage was 700 V, the scan speed was 1200 nm min^{-1}, the slit width of excitation and emission is 5 nm. In this paper, the **EuL** is selected as test sample for systematic research, owing to its higher yield than **TbL**. The strongest emission wavelengths for **EuL** were located at 616 nm when excited at 320 nm. For the experiment of sensing small organic molecules, the **EuL**–solvent emulsions were prepared by introducing 5 mg of **EuL** powder into 5.00 mL of methanol, ethanol, 2-propanol, acetone, acetonitrile, chloroform, DMF and THF, benzene, methylbenzene, *p*-xylene, chlorobenzene, 1-phenylethanone, and benzaldehyde, respectively; for the experiment of sensing metal ions, the **EuL**–solvent emulsions were prepared by introducing 5 mg of **EuL** powder into 5.00 mL of $M(NO_3)_x$ ($M = Na^+$, K^+, Mg^{2+}, Ca^{2+}, Mn^{2+}, Cd^{2+}, Zn^{2+},Co^{2+}, Cu^{2+}, Gd^{3+}) DMF solution for the luminescence studies.

Table 2 Selected bond lengths and angles for **EuL** and **TbL**[a,b]

Compound **EuL**			
Eu(1)–O(5)	2.353(6)	Eu(1)–O(2)	2.365(6)
Eu(1)–O(6)	2.394(6)	Eu(1)–O(8)	2.414(8)
Eu(1)–O(7)	2.438(10)	Eu(1)–O(1)$^{\#1}$	2.448(6)
Eu(1)–O(4)	2.458(6)	Eu(1)–O(3)	2.521(7)
Eu(1)–O(5)$^{\#2}$	2.717(6)	O(5)–Eu(1)$^{\#2}$	2.717(6)
O(1)–Eu(1)$^{\#3}$	2.448(6)		
O(5)–Eu(1)–O(2)	74.4(2)	O(5)–Eu(1)–O(6)	80.5(2)
O(2)–Eu(1)–O(6)	132.8(2)	O(5)–Eu(1)–O(8)	81.9(2)
O(2)–Eu(1)–O(8)	138.2(3)	O(6)–Eu(1)–O(8)	74.0(3)
O(5)–Eu(1)–O(7)	149.4(3)	O(2)–Eu(1)–O(7)	135.9(3)
O(6)–Eu(1)–O(7)	73.8(3)	O(8)–Eu(1)–O(7)	75.3(4)
O(5)–Eu(1)–O(1)$^{\#1}$	124.3(2)	O(2)–Eu(1)–O(1)$^{\#1}$	72.7(2)
O(6)–Eu(1)–O(1)$^{\#1}$	90.5(2)	O(8)–Eu(1)–O(1)$^{\#1}$	147.5(2)
O(7)–Eu(1)–O(1)$^{\#1}$	73.0(4)	O(5)–Eu(1)–O(4)	129.6(2)
O(2)–Eu(1)–O(4)	76.1(2)	O(6)–Eu(1)–O(4)	146.7(2)
O(8)–Eu(1)–O(4)	94.4(3)	O(7)–Eu(1)–O(4)	73.0(3)
O(1)$^{\#1}$–Eu(1)–O(4)	83.0(2)	O(5)–Eu(1)–O(3)	80.6(2)
O(2)–Eu(1)–O(3)	71.4(2)	O(6)–Eu(1)–O(3)	142.2(2)
O(8)–Eu(1)–O(3)	71.1(3)	O(7)–Eu(1)–O(3)	110.2(3)
O(1)$^{\#1}$–Eu(1)–O(3)	127.1(2)	O(4)–Eu(1)–O(3)	51.5(2)
O(5)–Eu(1)–O(5)$^{\#2}$	76.2(2)	O(2)–Eu(1)–O(5)$^{\#2}$	67.7(2)
O(6)–Eu(1)–O(5)$^{\#2}$	67.9(2)	O(8)–Eu(1)–O(5)$^{\#2}$	138.4(2)
O(7)–Eu(1)–O(5)$^{\#2}$	108.2(3)	O(1)$^{\#1}$–Eu(1)–O(5)$^{\#2}$	50.08(19)
O(4)–Eu(1)–O(5)$^{\#2}$	126.7(2)	O(3)–Eu(1)–O(5)$^{\#2}$	137.0(2)
Compound **TbL**			
Tb(1)–O(4)$^{\#4}$	2.318(7)	Tb(1)–O(2)	2.338(7)
Tb(1)–O(8)	2.365(9)	Tb(1)–O(1)$^{\#4}$	2.375(7)
Tb(1)–O(3)	2.412(7)	Tb(1)–O(7)	2.420(9)
Tb(1)–O(5)	2.437(7)	Tb(1)–O(6)	2.503(8)
Tb(1)–O(4)	2.729(7)	O(1)–Tb(1)$^{\#4}$	2.375(7)
O(4)–Tb(1)$^{\#4}$	2.318(7)		
O(4)$^{\#4}$–Tb(1)–O(2)	74.9(2)	O(4)$^{\#4}$–Tb(1)–O(8)	81.9(3)
O(2)–Tb(1)–O(8)	138.6(3)	O(4)$^{\#4}$–Tb(1)–O(1)$^{\#4}$	80.6(2)
O(2)–Tb(1)–O(1)$^{\#4}$	132.8(3)	O(8)–Tb(1)–O(1)$^{\#4}$	74.4(3)
O(4)$^{\#4}$–Tb(1)–O(3)	124.6(2)	O(2)–Tb(1)–O(3)	73.1(3)
O(8)–Tb(1)–O(3)	146.7(3)	O(1)$^{\#4}$–Tb(1)–O(3)	89.4(3)
O(4)$^{\#4}$–Tb(1)–O(7)	148.9(3)	O(2)–Tb(1)–O(7)	135.9(3)
O(8)–Tb(1)–O(7)	74.6(4)	O(1)$^{\#4}$–Tb(1)–O(7)	73.7(3)
O(3)–Tb(1)–O(7)	73.0(3)	O(4)$^{\#4}$–Tb(1)–O(5)	129.9(2)
O(2)–Tb(1)–O(5)	75.7(3)	O(8)–Tb(1)–O(5)	94.6(3)
O(1)$^{\#4}$–Tb(1)–O(5)	146.6(3)	O(3)–Tb(1)–O(5)	83.0(3)
O(7)–Tb(1)–O(5)	73.0(3)	O(4)$^{\#4}$–Tb(1)–O(6)	80.4(3)
O(2)–Tb(1)–O(6)	71.0(3)	O(8)–Tb(1)–O(6)	71.6(3)
O(1)$^{\#4}$–Tb(1)–O(6)	142.8(3)	O(3)–Tb(1)–O(6)	127.5(3)
O(7)–Tb(1)–O(6)	110.3(3)	O(5)–Tb(1)–O(6)	51.9(3)
O(4)$^{\#4}$–Tb(1)–O(4)	76.1(2)	O(2)–Tb(1)–O(4)	67.6(2)
O(8)–Tb(1)–O(4)	138.6(3)	O(1)$^{\#4}$–Tb(1)–O(4)	67.7(2)
O(3)–Tb(1)–O(4)	50.2(2)	O(7)–Tb(1)–O(4)	108.8(3)

[a] Symmetry codes: ($^{\#1}$) $-x+1/2, y+1/2, -z-1/2$; ($^{\#2}$) $-x+1/2, -y+3/2, -z$; ($^{\#3}$) $-x+1/2, y-1/2, -z-1/2$. [b] Symmetry codes: ($^{\#4}$) $-x+1/2, -y+3/2, -z+1$.

3 Results and discussion

3.1 Structure description

Single-crystal X-ray diffraction analysis reveals that the polymer consists of 2′-fluoro-biphenyl-3,4′,5-tricarboxylate (FBPT), lanthanide atom, coordinated H_2O and DMF molecules (Fig. 1a). **EuL** and **TbL** are isostructural and crystallize in the monoclinic space group *C*2/*c*. In the **EuL**, the Eu^{3+} ion is nine coordinated by seven oxygen atoms from the carboxyl groups of FBPT, one oxygen atom (O8) from DMF and one oxygen atom (O7) from the terminal water molecule, forming a distorted tricapped trigonal prism. The average Eu–O bond length is 2.565 Å within a range of 2.353–2.717 Å (2.318–2.729 Å in **TbL**) (Table 2). The bond angles for O–Eu–O are in the range of 50.1–149.4° (50.2–148.9° in **TbL**) (Table 2). All O–Eu–O bond angles and Eu–O bond lengths are within the expected ranges.

Notably, further study into the structure of **EuL** (or **TbL**) showed that the compound was a three-dimensional (3D) open framework. A better insight into the nature of the intricate framework can be achieved by the application of a topological approach, which is necessary to simplify the building blocks. As shown in Fig. 2, each $[FBPT]^{3-}$ ligand can be considered as a three-connecting node since it links three binuclear-Eu units and each binuclear-Eu unit in turn links six $[FBPT]^{3-}$ ligands, which can be regarded as a six-connecting node. The resulting (3,6)-connected net resembles the fluorite structure with the Schläfli symbol of $(4^2\cdot6)_2(4^4\cdot6^2\cdot8^7\cdot10^2)$. What is most interesting is that one-dimensional (1D) ellipsoidal shaped channels exist along the *c* axis (Fig. 1b). As shown in Fig. 1c and d, water molecules and fluorine atoms, which can be the potential sites for their sensing functions of small organic molecules, or metal ions are regularly distributed in the channel. The solvent-accessible volume of 1317.3 $Å^3$ out of the 4666.2 $Å^3$ unit cell volume (28.2% of the total crystal volume), calculated by PLATON, and the moderate pore sizes indicating such 1D channels are accessible to a variety of small organic molecules or metal ions.[16]

3.2 Gas and I_2 sorption

To examine the existence of the 1D channel, gas and I_2 sorption were studied. The **EuL** was activated at a temperature of 120 °C under vacuum for gas sorption studies. As shown in Fig. S3 and

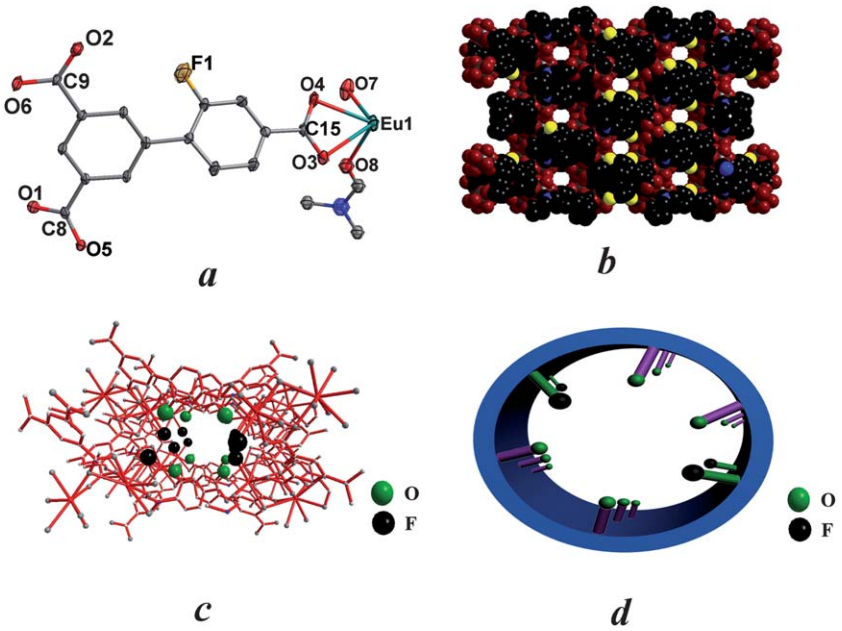

Fig. 1 (a) ORTEP representation of compound **EuL** (hydrogen atoms were omitted for clarity), (b) the space-filling view of **EuL** along the *c* axis, (c) a view of the one-dimensional channel structure, and (d) a schematic illustration of the one-dimensional channel structure.

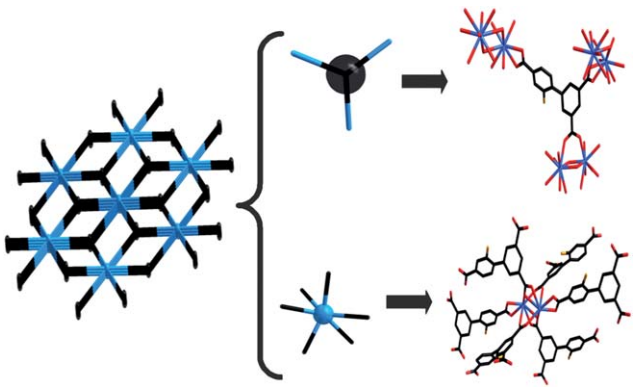

Fig. 2 Schematic illustration of the topology of the 3D network of **EuL** (black and blue balls represent three-connected FBPT ligands and six-connected paddle-wheel building blocks, respectively).

S4,† both the N_2 and H_2 sorption isotherm at 77 K show that there is certain porosity in the compound of **EuL**. According to the reported literature, the experiment of I_2 sorption is also a very good and effective way to verify the existence of micro-sized pores.[17] As shown in Fig. 3, when the outgassed sample of **EuL** (100 mg) was immersed in a hexane (10 mL) solution of I_2 (0.1 mol L^{-1}), the color of the crystals intensified from pale yellow to brown gradually. Notably, the photographs and XRD for **EuL** releasing I_2, demonstrate that the I_2 sorption progress of **EuL** is reversible. Besides, the TG curve of I_2-incorporated **EuL** shows a hysteresis for the loss of the iodine, suggesting that there are some interactions between the guest molecules and the framework (Fig. S5†). Undoubtedly, the experiment of I_2 sorption provides additional proof of the 1D channel for the compound **EuL**.

3.3 Thermal stability

In order to examine the thermal stability of **EuL** and **TbL**, thermal gravimetric analyses (TGA) (Fig. 4) were studied from 46 to 900 °C. The TGA diagrams of the two compounds are quite similar, and both show two main weight losses in the curves. In **EuL**, the TGA curve shows that the first weight loss was at 13.82% in the temperature range 46–255 °C, corresponding to the loss of DMF and water molecules (calculated value of 14.17%). The second weight loss was at 56.01% from 445 to 505 °C, ascribed to the release of the ligand composite (calculated value of 55.34%). For compound **EuL**, the final product was Eu_2O_3, which is confirmed by PXRD studies. The weight loss of compound **TbL** with the increase of temperature is similar to **EuL**, and both fit well with the calculated value.

3.4 Sensing of small organic molecules

To examine the potential of the **EuL** for the sensing of small molecules, the compound was immersed in methanol, ethanol, 2-propanol, acetone, acetonitrile, chloroform, DMF and THF solvent emulsions for luminescence studies. The emission spectra of **EuL** excited at 320 nm reveals the well-resolved magnified luminescence of the f–f transitions, attributed to the energy transfer from FBPT ligands to Eu^{3+}. Characteristic transitions of the Eu^{3+} ion are also evident for **EuL**, at 590, 616, 651 and 698 nm, which are ascribed to the $^5D_0 \rightarrow {}^7F_1$, $^5D_0 \rightarrow {}^7F_2$, $^5D_0 \rightarrow {}^7F_3$ and $^5D_0 \rightarrow {}^7F_4$ transitions, respectively. As shown in Fig. 5, the photoluminescence (PL) intensity is largely dependent on the solvent molecules, especially in the case of acetone, which showed a significant quenching effect. The **EuL** were dispersed in DMF as the standard suspension, while the acetone content was gradually increased to monitor the emissive response. As shown in Fig. 6, the luminescent intensity of

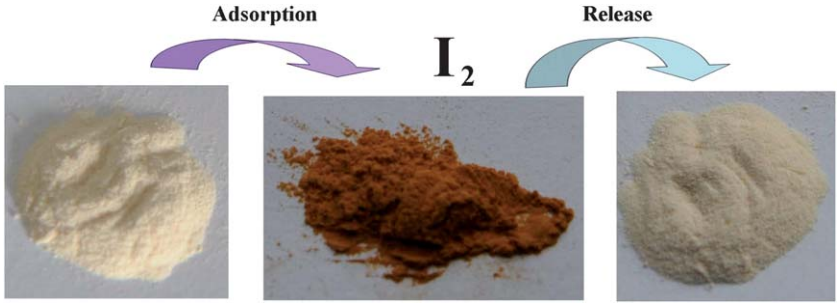

Fig. 3 Photographs of **EuL** for the adsorption and release of I_2. For adsorption, the outgassed sample of **EuL** (100 mg) was immersed in a hexane (10 mL) solution of I_2 (0.1 mol L^{-1}). For release, the sample of I_2–**EuL** was soaked in 20 mL hexane, and replaced hexane (20 mL) per 20 min over 8 h.

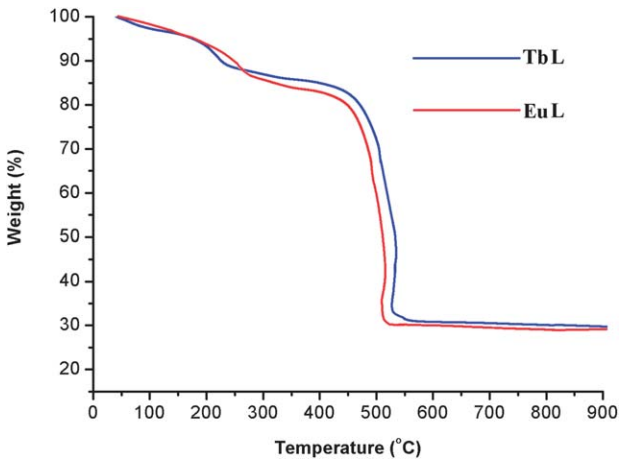

Fig. 4 Thermal gravimetric analyses curves for **EuL** and **TbL**.

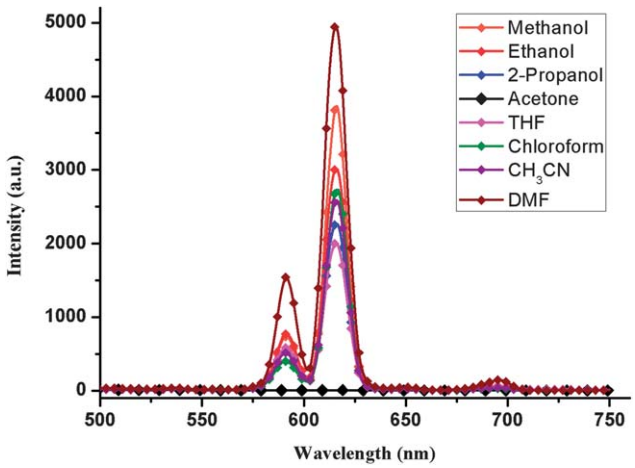

Fig. 5 PL spectra of **EuL** introduced into methanol, ethanol, 2-propanol, acetone, THF, chloroform, CH_3CN and DMF.

the suspension significantly decreased with the addition of acetone, and it almost disappeared at an acetone content of 5.0 vol%. This decreasing trend of the luminescent intensity may be significant to identify the presence of small amounts of acetone in solution. Besides, the decreasing trend of the luminescent intensity of the $^5D_0 \rightarrow {}^7F_2$ transition of Eu^{3+} at 616 nm *versus* the volume ratio of acetone could be well fitted with a first-order exponential decay (Fig. S7†), indicating that luminescence quenching of **EuL** by acetone is diffusion-controlled.[13e]

Such solvent-dependent luminescence properties are very interesting and important for the selective sensing of solvent molecules. The above results evoked by the acetone solvent molecules, led us to an exploration of more small organic molecules. As shown in Fig. 7, the solvents used were benzene, methylbenzene, *p*-xylene, chlorobenzene, 1-phenylethanone and benzaldehyde, and all of them have an aromatic ring. **EuL** has been demonstrated to show a selective sieving function with respect to 1-phenylethanone and benzaldehyde. When the 1-phenylethanone or benzaldehyde solvent content was gradually added and increased to the **EuL** DMF standard emulsion, the luminescent intensity also gradually decreased with the addition of 1-phenylethanone or benzaldehyde.

Powder XRD was employed to study the structural data of the original and exchanged compounds. The powder XRD pattern of the acetone–**EuL**, 1-phenylethanone–**EuL**, and benzaldehyde–**EuL** are similar to that of **EuL**, suggesting that the basic frameworks remain in the compounds (Fig. S6†). In the solvents we used, acetone, 1-phenylethanone and benzaldehyde all have a strong absorbing range from 250 to 350 nm, while other

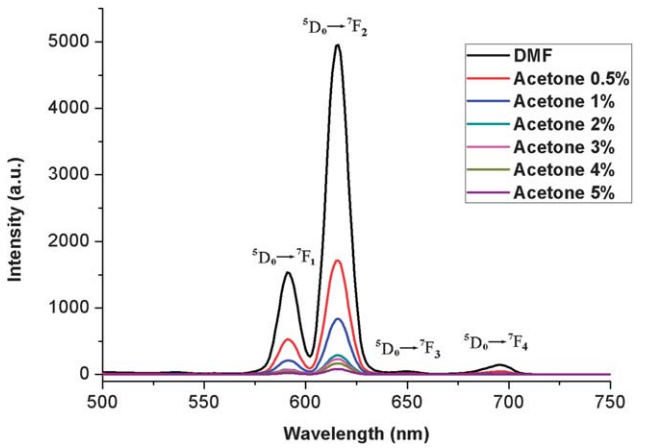

Fig. 6 The PL spectra of **EuL** DMF emulsion in the presence of various contents of acetone solvent.

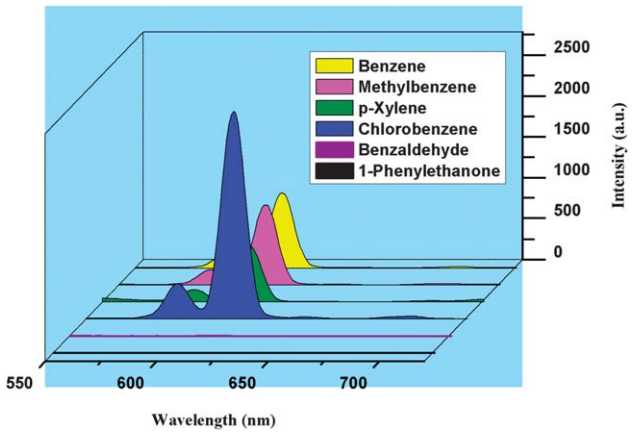

Fig. 7 PL spectra of **EuL** introduced into benzene, methylbenzene, *p*-xylene, chlorobenzene and 1-phenylethanone.

solvents have no significant absorption band in this range. As shown in Fig. 8, the strong absorption band of FBPT is located from 250 to 310 nm, which is largely overlapped by the absorbing band of acetone (1-phenylethanone or benzaldehyde). The physical interaction of the solute and solvent plays an important role in such luminescence quenching effects of small solvent molecules. Upon excitation, there is competition of the absorption of the light source energy between acetone (1-phenylethanone or benzaldehyde) molecules and FBPT from 250 to 310 nm. Combined with the absorption and luminescent spectra, it was suggested that the energy absorbed by the FBPT is transferred to the acetone (1-phenylethanone or benzaldehyde) molecules, resulting in a decrease in the luminescence intensity, even quenching, of **EuL**. The quenching mechanism is in agreement with that proposed previously by Chen *et al.*[14d,18]

3.5 Sensing of metal ions

The **EuL** was immersed in DMF solutions containing $M(NO_3)_x$ ($M = Na^+$, K^+, Mg^{2+}, Ca^{2+}, Mn^{2+}, Cd^{2+}, Zn^{2+},Co^{2+}, Cu^{2+}, Gd^{3+}) to form metal-ion-incorporated **EuL** as microcrystalline solids for luminescence studies. The PL spectra of Cu^{2+}-incorporated **EuL** are shown in Fig. 10, and exhibit typical Eu^{3+} ion transitions. The most important feature is that the luminescence intensities of the different suspensions are strongly dependent on the identities of the metal ions. Zn^{2+}, Mg^{2+}, Ca^{2+}, Cd^{2+}, Gd^{3+} ions, possessing a closed-shell electron configuration, have a trivial effect on the luminescence intensity, whereas the other metal ions with different electron configurations produce varying degrees of quenching of the luminescence intensity, especially the Cu^{2+} ion (Fig. 9). The emitted visible red light of the **EuL** suspension containing Cu^{2+} ion is significantly darker than the original one under UV light (Fig. 10), which allowed us to identify easily the existence of a small amount of Cu^{2+} ion in DMF solution. It is very remarkable that this material features such highly selective and sensitive sensing of Cu^{2+} ion in DMF solution.

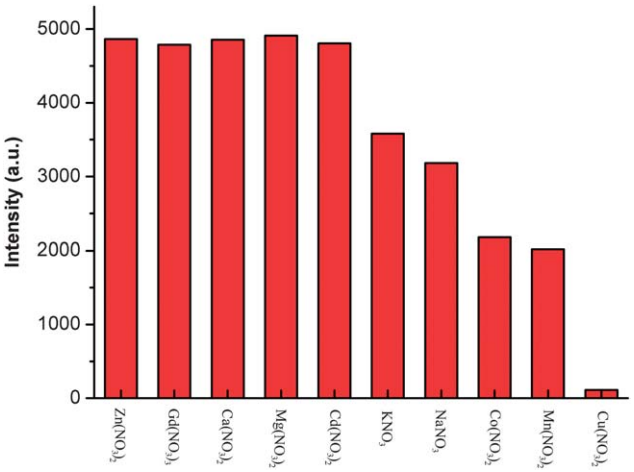

Fig. 9 A comparison of the luminescence intensities of the $^5D_0 \rightarrow {}^7F_2$ transitions of **EuL** exchanging with 0.01 M DMF solution with different metal ions.

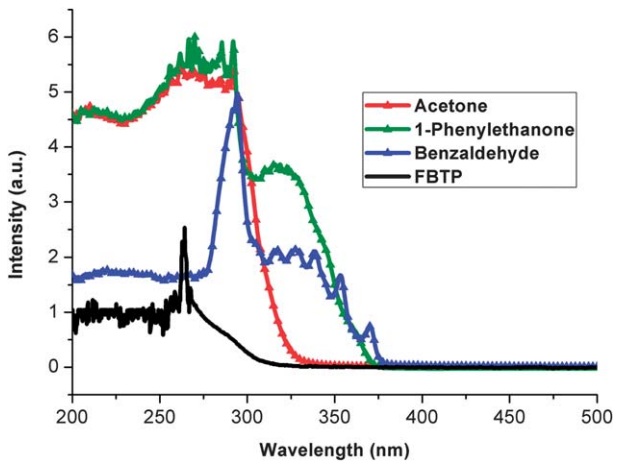

Fig. 8 The UV/vis absorption spectra for acetone, 1-phenylethanone, benzaldehyde and FBPT.

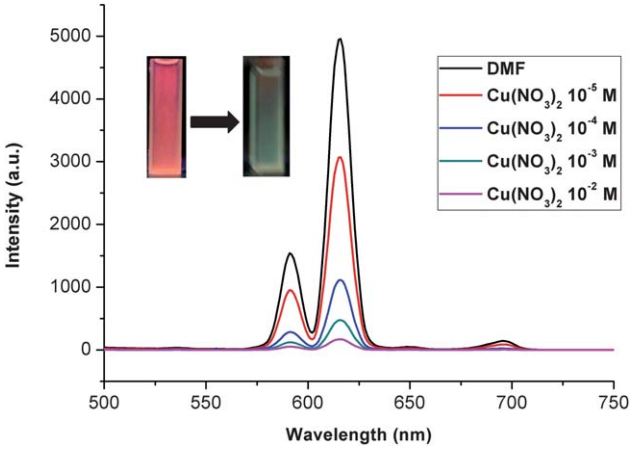

Fig. 10 The PL spectra of **EuL** in $Cu(NO_3)_2$ DMF solution at different concentrations. The inset shows the luminescence change after the addition of Cu^{2+} ion in **EuL** suspension under UV light.

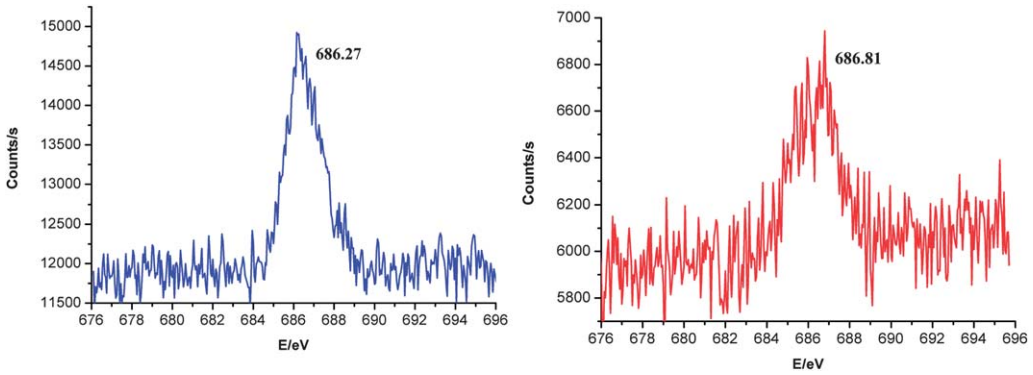

Fig. 11 F1s X-ray photoelectron spectroscopy (XPS) spectra of the **EuL** (blue) and Cu^{2+}-incorporated **EuL** (red).

According to the reported literature, the examples of porous MOFs with Lewis basic sites, such as pyridyl sites,[13d,19] amide sites,[20] anionic sulfonate sites,[21] and so on, could have an effect on metal ions. As for the reason of the quenching by Cu^{2+}, we speculate that it might be related to the interaction between the Cu^{2+} ions and the fluorine, carboxylate and/or terminal water Lewis basic sites on the **EuL**, similar to that observed in the reported literature.[14c,22] The interaction between the Cu^{2+} ions and the FBPT ligands minimizes the energy transfer efficiency from FBPT to the Eu^{3+} ions within **EuL**, thus decreasing the luminescent intensity. To check the results, F1s X-ray photoelectron spectroscopy (XPS) was selected to study the **EuL** and Cu^{2+}-incorporated **EuL**. The F1s peak from free fluorine atoms at 686.27 eV in **EuL** is shifted to 686.81 eV on the addition of Cu^{2+} (Fig. 11), indicating the weak interaction of fluorine atoms with Cu^{2+} in the Cu^{2+}-incorporated **EuL**.

4 Conclusions

In conclusion, two new 3D lanthanide metal–organic frameworks were synthesized by means of solvothermal methods using fluorinated tricarboxylic acid as an organic ligand. These materials exhibited a one-dimensional channel structure in which fluorine atoms and coordinated water molecules are regularly distributed. **EuL** shows a remarkable quenching effect in the luminescence emission of Eu^{3+} upon the introduction of the small organic molecules (acetone, 1-phenylethanone and benzaldehyde) and Cu^{2+} ion. It is expected that the easy access to luminescent one-dimensional channel MOFs with a variety of organic solvents and metal ions will render this strategy very practical and useful in exploring luminescent microporous organic-molecule and metal-ion sensors. This research can be considered as a work that is devoted to the potential applications of Ln-MOFs, and further work on this theme is currently under way.

Acknowledgements

The authors are grateful to the financial aid from the National Natural Science Foundation of China (Grant nos 21071140, 91122030 and 21210001), 863'-National High Technology Research and Development Program of China (Grant no. 2011AA03A407) and National Natural Science Foundation for Creative Research Group (Grant no. 21221061).

Notes and references

1 (*a*) M. Eddaoudi, D. B. Moler, H. Li, B. Chen, T. M. Reineke, M. O'Keeffe and O. M. Yaghi, *Acc. Chem. Res.*, 2001, **34**, 319; (*b*) S. Kitagawa, R. Kitaura and S. I. Noro, *Angew. Chem., Int. Ed.*, 2004, **43**, 2334; (*c*) L. J. Murray, M. Dincă and J. R. Long, *Chem. Soc. Rev.*, 2009, **38**, 1294; (*d*) S. Ma and H. C. Zhou, *Chem. Commun.*, 2010, **46**, 44; (*e*) J. R. Li, R. J. Kuppler and H. C. Zhou, *Chem. Soc. Rev.*, 2009, **38**, 1477; (*f*) L. Ma, C. Abney and W. Lin, *Chem. Soc. Rev.*, 2009, **38**, 1248; (*g*) B. Chen, S. C. Xiang and G. Qian, *Acc. Chem. Res.*, 2010, **43**, 1115; (*h*) H. L. Jiang and Q. Xu, *Chem. Commun.*, 2011, **47**, 3351.

2 S. Chen, J. Zhang, T. Wu, P. Feng and X. Bu, *J. Am. Chem. Soc.*, 2009, **131**, 16027.

3 A. Lan, K. Li, H. Wu, D. H. Olson, T. J. Emge, W. Ki, M. C. Hong and J. Li, *Angew. Chem., Int. Ed.*, 2009, **48**, 2334.

4 S. Horike, D. Tanaka, K. Nakagawa and S. Kitagawa, *Chem. Commun.*, 2007, 3395.

5 Y. K. Hwang, D. Y. Hong, J. S. Chang, S. H. Jhung, Y. K. Seo, J. Kim, A. Vimont, M. Daturi, C. Serre and G. Férey, *Angew. Chem., Int. Ed.*, 2008, **47**, 4144.

6 Y. B. Zhang, W. X. Zhang, F. Y. Feng, J. P. Zhang and X. M. Chen, *Angew. Chem., Int. Ed.*, 2009, **48**, 5287.

7 G. Huang, C. Yang, Z. Xu, H. Wu, J. Li, M. Zeller, A. D. Hunter, S. S. Y. Chui and C. M. Che, *Chem. Mater.*, 2009, **21**, 541.

8 (*a*) J. Kido and Y. Okamoto, *Chem. Rev.*, 2002, **102**, 2357; (*b*) N. Marques, A. Sella and J. Takats, *Chem. Rev.*, 2002, **102**, 2137.

9 (*a*) M. D. Allendorf, C. A. Bauer, R. K. Bhakta and R. J. T. Houk, *Chem. Soc. Rev.*, 2009, **38**, 1330; (*b*) Y. J. Cui, Y. F. Yue, G. D. Qian and B. L. Chen, *Chem. Rev.*, 2012, **112**, 1126; (*c*) J. Rocha, L. D. Carlos, F. A. A. Paz and D. Ananias, *Chem. Soc. Rev.*, 2011, **40**, 926; (*d*) L. D. Carlos, R. A. S. Ferreira and S. J. L. Ribeiro, *Adv. Mater.*, 2009, **21**, 509; (*e*) K. Binnemans, *Chem. Rev.*, 2009, **109**, 4283.

10 (*a*) K. A. White, D. A. Chengelis, M. Zeller, S. J. Geib, J. Szakos, S. Petoud and N. L. Rosi, *Chem. Commun.*, 2009, 4506; (*b*) K. A. White, D. A. Chengelis, K. A. Gogick, J. Stehman, N. L. Rosi and S. Petoud, *J. Am. Chem. Soc.*, 2009, **131**, 18069; (*c*) H. L. Jiang, N. Tsumori and Q. Xu, *Inorg. Chem.*, 2010, **49**, 10001; (*d*) W. J. Rieter, K. M. L. Taylor, H. An, W. Lin and W. Lin, *J. Am. Chem. Soc.*, 2006, **128**, 9024; (*e*) Q. G. Meng, R. J. Witte, Y. J. Gong, E. L. Day, J. C. Chen, P. S. May and M. T. Berry, *Chem. Mater.*, 2010, **22**, 6056; (*f*) H. L. Guo, Y. Z. Zhu, S. L. Qiu, J. A. Lercher and H. J. Zhang, *Adv. Mater.*, 2010, **22**, 4190; (*g*) Y. J. Cui, G. D. Qian and B. L. Chen, *J. Am. Chem. Soc.*, 2012, **134**, 3979.

11 (*a*) S. I. Weissman, *J. Chem. Phys.*, 1942, **10**, 214; (*b*) F. J. Steemers, W. Verboom, D. N. Reinhoudt, E. B. van der Tol and J. W. Verhoeven, *J. Am. Chem. Soc.*, 1995, **117**, 9408.

12 (*a*) P. Horcajada, R. Gref, T. Baati, P. K. Allan and C. Serre, *Chem. Rev.*, 2012, **112**, 1232; (*b*) L. E. Kreno, M. Allendorf and J. T. Hupp, *Chem. Rev.*, 2012, **112**, 1105; (*c*) W. J. Rieter, K. M. L. Taylor and W. B. Lin, *J. Am. Chem. Soc.*, 2007, **129**, 9852; (*d*) K. Hanaoka, K. Kikuchi, H. Kojima, Y. Urano and T. Nagano, *Angew. Chem.*, 2003, **115**, 3104.

13 (*a*) W. Liu, T. Jiao, Y. Li, Q. Liu, M. Tan, H. Wang and L. Wang, *J. Am. Chem. Soc.*, 2004, **126**, 2280; (*b*) B. Chen, L. Wang, F. Zapata, G. Qian and E. B. Lobkovsky, *J. Am. Chem. Soc.*, 2008, **130**, 6718; (*c*) B. Chen, L. Wang, Y. Xiao, F. R. Fronczek, M. Xue, Y. Cui and G. Qian, *Angew. Chem., Int. Ed.*, 2009, **48**, 500; (*d*) B. V. Harbuzaru, A. Corma, F. Rey, P. Atienzar, J. L. Jordá, H. García, D. Ananias, L. D. Carlos and J. Rocha, *Angew. Chem., Int. Ed.*, 2008, **47**, 1080; (*e*) B. L. Chen, Y. Yang, F. Zapata, G. Lin, G. Qian and E. B. Lobkovsky, *Adv. Mater.*, 2007, **19**, 1693; (*f*) E. Y. Lee, S. Y. Jang and M. P. Suh, *J. Am. Chem. Soc.*, 2005, **127**, 6374.

14 (*a*) Z. Y. Guo, H. Xu, S. Q. Su, J. F. Cai, S. Dang, S. C. Xiang, G. D. Qian, H. J. Zhang, M. O'Keeffe and B. L. Chen, *Chem. Commun.*, 2011, **47**, 5551; (*b*) S. Dang, E. Ma, Z. S. Sun and H. J. Zhang, *J. Mater. Chem.*, 2012, **22**, 16920; (*c*) W. T. Yang, J. Feng and H. J. Zhang, *J. Mater. Chem.*, 2012, **22**, 6819; (*d*) W. T. Yang, J. Feng, S. Y. Song and H. J. Zhang, *ChemPhysChem*, 2012, **13**, 2734.

15 G. M. Sheldrick, *SHELXL-97, Program for Refinement of Crystal Structures*, University of Göttingen, Germany, 1997.

16 A. L. Spek, *J. Appl. Crystallogr.*, 2003, **36**, 7.

17 (*a*) Z. J. Zhang, W. Shi, Z. Niu, H. H. Li, B. Zhao, P. Cheng, D. Z. Liao and S. P. Yan, *Chem. Commun.*, 2011, **47**, 6425; (*b*) Q. K. Liu, J. P. Ma and Y. B. Dong, *Chem. Commun.*, 2011, **47**, 7185; (*c*) M. H. Zeng, Q. X. Wang, Y. X. Tan, S. Hu, H. X. Zhao, L. S. Long and M. Kurmoo, *J. Am. Chem. Soc.*, 2010, **132**, 2561; (*d*) Z. Yin, Q. X. Wang and M. H. Zeng, *J. Am. Chem. Soc.*, 2012, **134**, 4857.

18 Y. Q. Xiao, L. B. Wang, Y. J. Cui, B. L. Chen, F. Zapata and G. D. Qian, *J. Alloys Compd.*, 2009, **484**, 601.

19 J. S. Seo, D. Whang, H. Lee, S. I. Jun, J. Oh, Y. J. Jeon and K. Kim, *Nature*, 2000, **404**, 982.

20 S. Hasegawa, S. Horike, R. Matsuda, S. Furukawa, K. Mochizuki, Y. Kinoshita and S. Kitagawa, *J. Am. Chem. Soc.*, 2007, **129**, 2607.

21 S. Horike, S. Bureekaew and S. Kitagawa, *Chem. Commun.*, 2008, 471.

22 Y. Q. Xiao, Y. J. Cui, Q. Zheng, S. C. Xiang, G. D. Qian and B. L. Chen, *Chem. Commun.*, 2010, **46**, 5503.

